Separation of experimental 2D IR frequency-frequency correlation functions into structural and reorientation-induced contributions

Patrick L. Kramer,[a] Jun Nishida,[a] and Michael D. Fayer[b]
Department of Chemistry, Stanford University, Stanford, California 94305, USA

(Received 30 July 2015; accepted 8 September 2015; published online 28 September 2015)

A vibrational transition frequency can couple to its environment through a directional vector interaction. In such cases, reorientation of the vibrational transition dipole (molecular orientational relaxation) and its frequency fluctuations can be strongly coupled. It was recently shown [Kramer *et al.*, J. Chem. Phys. **142**, 184505 (2015)] that differing frequency-frequency correlation function (FFCF) decays, due to reorientation-induced spectral diffusion (RISD), are observed with different two-dimensional infrared polarization configurations when such strong coupling is present. The FFC functional forms were derived for the situation in which all spectral diffusion is due to reorientational motion. We extend the previous theory to include vibrational frequency evolution (spectral diffusion) caused by structural fluctuations of the medium. Model systems with diffusive reorientation and several regimes of structural spectral diffusion rates are analyzed for first order Stark effect interactions. Additionally, the transition dipole reorientational motion in complex environments is frequently not completely diffusive. Several periods of restricted angular motion (wobbling-in-a-cone) may precede the final diffusive orientational randomization. The polarization-weighted FFCF decays are presented in this case of restricted transition dipole wobbling. With these extensions to the polarization-dependent FFCF expressions, the structural spectral diffusion dynamics of methanol in the room temperature ionic liquid 1-hexyl-3-methylimidazolium hexafluorophosphate can be separated quantitatively from RISD using the experimental center line slope data. In addition, prior results on the spectral diffusion of water, methanol, and ethanol in 1-ethyl-3-methylimidazolium bis(trifluoromethylsulfonyl)imide are re-examined to elucidate the influence of reorientation on the data, which were interpreted in terms of structural fluctuations. © *2015 AIP Publishing LLC.* [http://dx.doi.org/10.1063/1.4931402]

I. INTRODUCTION

Measurement of spectral fluctuations by two-dimensional infrared (2D IR) vibrational echo spectroscopy provides a useful window into the structural dynamics of complex condensed phase media.[1–9] The inhomogeneous broadening of a vibrational transition reports on the range of environments and interactions experienced by a probe molecule of interest. Spectral diffusion within this inhomogeneous line shape is caused by various molecular motions in the medium that alter the probe's local environment and interactions, and therefore change its instantaneous vibrational frequency. The rates and fluctuation amplitudes of spectral diffusion processes are quantified by the frequency-frequency correlation function (FFCF), defined by

$$C(t) = \langle \delta\omega(0)\,\delta\omega(t)\rangle, \tag{1}$$

where $\delta\omega(t) = \omega(t) - \langle\omega\rangle$ is the instantaneous frequency fluctuation. The angle brackets $\langle\cdots\rangle$ are most commonly used to refer to an isotropic ensemble average, in which all frequency fluctuations are weighted equally.

A FFCF determines the waiting-time-dependent two-dimensional line shape observed in 2D IR spectroscopy,[1,10] but it need not be the isotropically averaged function in Eq. (1). The experiments are conducted using polarized laser pulses, which we will take to be linearly polarized. Each pulse interacts with a subset of the vibrational probe transition dipoles in the excitation volume. The probability of each field-dipole interaction is proportional to $\hat{\varepsilon}\cdot\hat{\mu}$, with $\hat{\varepsilon}$ and $\hat{\mu}$ the unit vectors of the laser electric field and molecular transition dipole, respectively. Thus, a general 2D IR pulse sequence, with three incident pulses that overlap in the sample and a local oscillator pulse for heterodyne detection (which must match the polarization of the emitted signal field),[2] interrogates an ensemble of molecular transition dipoles weighted by their overlap with the laser fields at the various interaction times of the pulse sequence.

Through techniques such as the center line slope (CLS) method,[3,4,11] the FFCF of the ensemble responsible for the third order nonlinear signal may be extracted from experimental 2D IR spectra. In principle, the ensembles observed when using two different combinations of excitation beam and detection polarizations (referred to as a polarization configuration) may display somewhat different spectral diffusion dynamics. Indeed, recently it was found that the CLS decays of the hydrogen bonded solute methanol-d_4 in a room temperature ionic liquid (RTIL), 1-hexyl-3-methylimidazolium hexafluorophosphate ($HmimPF_6$), varied significantly depending on the polarization configurations examined, $\langle XXXX\rangle$, $\langle XXYY\rangle$, and $\langle XYXY\rangle$.[12] Here, the $\langle ABCD\rangle$ tensor element refers to nonlinear

[a] P. L. Kramer and J. Nishida contributed equally to this work.
[b] Author to whom correspondence should be addressed. Electronic mail: fayer@stanford.edu

signal detected at *A* polarization after time ordered interactions with pulses 1–3 polarized at *D*, *C*, and *B*, respectively.

It was found that, if the interaction of the vibrational transition dipole with its surroundings transforms as a vector with dipole rotation, rather than a scalar, then reorientation-induced spectral diffusion (RISD) can contribute to the total CLS decay and cause different recorded dynamics with each polarization configuration.[12,13] The first order Stark effect was used as a model for such vector interactions, and, by assuming diffusive reorientation of the vibrational transition dipole, the polarization-weighted frequency-frequency correlation function (PW-FFCF) was calculated for both the $\langle XXXX\rangle$ (parallel polarized) and $\langle XXYY\rangle$ (perpendicular polarized) configurations. In agreement with experiment, the $\langle XXYY\rangle$ FFCF was predicted to decay more rapidly than that for $\langle XXXX\rangle$.

Qualitatively, the influence of reorientation on spectral diffusion can be understood as follows. Consider a vibrational transition of a molecular probe molecule that has its frequency at least in part determined by its interaction with electric fields internal to the sample through the Stark effect,[14,15] with a non-negligible electric field component that is static on the time scale of the orientational relaxation (see Figure 1). The Stark coupling depends on the difference in dipole moment between the vibrational excited state and ground state, which is taken to be parallel to the transition dipole. Then, as the molecule rotates, the transition dipole direction changes relative to the long lived electric field component, altering the vibrational frequency. For the parallel configuration, molecules will tend to be excited with the same polarization that gives rise to the signal. As they rotate, their frequencies will change, but they will rotate into directions that contribute less to the signal, as shown in Figure 1. Therefore, the RISD will be somewhat mitigated by the reduction in the contribution of the reoriented molecules to the detected 2D IR signal. For the perpendicular configuration $\langle XXYY\rangle$, molecules will be initially excited with their transition dipoles in directions that tend to have large components perpendicular to the signal polarization. As they rotate, their frequencies change and their transition dipoles will tend to move toward the signal polarization. Therefore, as rotation changes their frequency, they also contribute more to the 2D IR signal, amplifying their contribution to RISD. The result is that RISD in $\langle XXYY\rangle$ makes a greater contribution, resulting in faster spectral diffusion than in $\langle XXXX\rangle$.

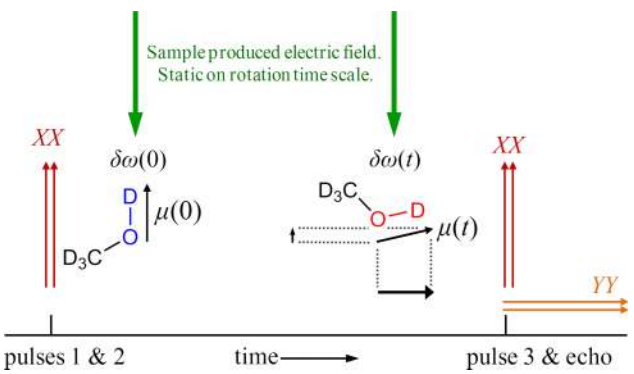

FIG. 1. Illustration of the RISD process, reorientation induced spectral diffusion, for one methanol-d_4 molecule in solution. The molecule experiences a long-lived electric field that, through the Stark effect, is in part responsible for inhomogeneous broadening. Rotation of the molecule changes the projection of the static electric field on the transition dipole (μ), changing the frequency. But the contribution of the frequency change to $\langle XXXX\rangle$ is reduced while the contribution to $\langle XXYY\rangle$ is increased.

The theory and model system considered previously[12] are not sufficient to quantitatively interpret experimental data because two major characteristics of many real condensed-phase systems were neglected. First, structural fluctuations in the vibrational probe's surroundings can modulate the coupling of the environment to the transition. The resulting structural spectral diffusion (SSD) does not depend on the polarization configuration and can increase the decay rate of all polarization-weighted FFCFs considerably.[12] Second, the reorientation dynamics are frequently more complex than free diffusion.[16,17] For example, in room temperature ionic liquids, the reorientation of a hydroxyl on dilute water and alcohol solutes has been observed to proceed by a hierarchy of progressively slower motions: a near-instantaneous inertial orientational jump, at least one period of restricted angular diffusion (wobbling-in-a-cone),[16,17] and finally complete diffusive orientational randomization.[18]

In the present work, structural spectral diffusion and restricted angular motion are incorporated into the first order Stark effect model of RISD.[12] In Section II, we prove that the FFCF decay can be factorized into a RISD part and a SSD part. Based on the derivation, the effect of reorientational frequency sampling on the observation of short and long time scale components of the structural degrees of freedom is examined, both for a freely diffusing transition dipole (Section III A) and for a dipole with an initial period of wobbling-in-a-cone followed by free diffusion (Sections III B and III C). It will be shown that when the SSD decay occurs on a much faster time scale than RISD, the structural contribution is barely affected, yielding similar FFCFs for the parallel and perpendicular polarizations. As the RISD time scale becomes faster relative to the SSD components, the FFCF is significantly accelerated by RISD, and the different polarization schemes become clearly distinguishable as well. These model cases will help characterize the potential appearance of RISD in experimental data. In Section IV A, using the complete model of the FFCF, SSD with RISD, the parallel and perpendicular CLS decays of methanol in $HmimPF_6$ can be separated into their distinct reorientational components and the structural dynamics which are purely a property of the system. Previously published spectral diffusion results[18] on water, methanol, and ethanol in the RTIL 1-ethyl-3-methylimidazolium bis(trifluoromethylsulfonyl)imide ($EmimNTf_2$) are also re-examined in Section IV B to determine the extent of possible RISD influence. Concluding remarks appear in Section V. An orthogonality condition necessary for the factorization of the FFCF is proved in Appendix A. The method of obtaining decay time constants for the wobbling-in-a-cone orientational correlation functions is summarized in Appendix B.

II. FFCF FACTORIZATION INTO SSD AND RISD COMPONENTS

We assume the vibrational transition dipole is engaged in a directional interaction, whose form is equal to that of the first

order Stark effect. Assignment of the fluctuating frequency to a time-varying Stark effect has been successful in the interpretation of spectral diffusion for a variety of vibrational probes.[14,19] Even if the vibrational frequency is not strictly determined by a Stark effect, a strongly directional interaction can be modeled using the electric field along the dipole as a surrogate for the generally more complex intermolecular interactions, with a suitably chosen effective Stark tuning rate (often referred to as a frequency map).[20–23]

In this case, the frequency fluctuation will transform as a vector as the dipole reorients relative to the lab frame (in which the laser field polarizations are fixed). We can write the vector frequency fluctuation as[12]

$$\delta\omega_v(t) = \lambda\vec{E}(t)\cdot\hat{\mu}(t), \tag{2}$$

where $\hat{\mu}$ is the unit vector parallel to the transition dipole and dipole difference for the transition, $\vec{E}$ is the internal sample electric field at the position of the molecular dipole, and λ is the Stark tuning rate. If E is the field amplitude and $\hat{e}$ is the unit vector specifying its direction, Eq. (2) then becomes

$$\delta\omega_v(t) = \lambda E(t)\hat{e}(t)\cdot\hat{\mu}(t) = \lambda E(t)\cos(\theta_F(t)), \tag{3}$$

with θ_F the angle between the electric field and the transition dipole.[12] In general, both the field amplitude and direction can vary due to the fluctuations of the medium surrounding the vibrational probe. However, we assume that these structural fluctuations are uncorrelated with the transition dipole direction.

All spectral diffusion dynamics which depend on the transition dipole direction are contained in the vector frequency fluctuation $\delta\omega_v$. Isotropic structural dynamics such as density fluctuations may also cause the frequency to fluctuate without affecting the vector coupling.[24] We represent such dynamics by the scalar frequency fluctuation, $\delta\omega_s$. Therefore, the total time-dependent frequency fluctuation is

$$\delta\omega(t) = \delta\omega_v(t) + \delta\omega_s(t). \tag{4}$$

As discussed in Section I, the nature of laser pulse spectroscopy with polarized beams implies that ensemble averages involving the vector frequency fluctuation will depend on the polarization configuration. If p denotes the polarization configuration, we define $\langle\cdots\rangle_p$ as an ensemble average with weighting according to p and the transition dipole orientational dynamics. The p-configuration polarization-weighted FFCF is, therefore,

$$C_p(t) = \langle\delta\omega(t)\,\delta\omega(0)\rangle_p = \langle\delta\omega_v(t)\,\delta\omega_v(0)\rangle_p + \langle\delta\omega_s(t)\,\delta\omega_s(0)\rangle_p + 2\langle\delta\omega_v(t)\,\delta\omega_s(0)\rangle_p. \tag{5}$$

We consider the final term, and note that

$$\langle\delta\omega_v(t)\,\delta\omega_s(0)\rangle_p = \lambda\langle\delta\omega_s(0)\,E(t)\,\hat{e}(t)\rangle_p\cdot\langle\hat{\mu}(t)\rangle_p = 0 \tag{6}$$

because $\langle\hat{\mu}(t)\rangle_p = 0$, that is, the transition dipole direction is random with respect to both the local E-fields and lab frame. Note that while certain dipole orientations are preferred due to the polarization weighting, the reversed directions are equally likely and hence the average must be zero. Additionally, because $\delta\omega_s$ is a scalar, the polarization-weighted correlation function of this term is identical to an isotropically averaged correlation function. Thus, we write

$$C_p(t) = \langle\delta\omega_v(t)\,\delta\omega_v(0)\rangle_p + \langle\delta\omega_s(t)\,\delta\omega_s(0)\rangle = C_v^p(t) + C_s(t). \tag{7}$$

The overall PW-FFCF $C_p(t)$ is therefore a sum of a vector FFCF $C_v^p(t)$, which is dependent on the polarization configuration p, and a scalar FFCF $C_s(t)$, which is always given by an isotropic ensemble average. The scalar FFCF will be discussed later (Section IV A); the main focus of this paper will be on the vector FFCF, because it is this term that reports on reorientation-induced spectral diffusion.

The first order Stark model treated previously involved an internal sample electric field that is static in both amplitude and orientation during the rotational dynamics of the transition dipole being studied.[12] The field amplitude was assumed to be equal at each dipole position, but the initial orientations of the field and transition dipole unit vectors were randomized in the polarization-weighted ensemble averaging procedure. Only vector coupling was considered, so the frequency fluctuation was

$$\delta\omega(t) = \lambda E\hat{e}\cdot\hat{\mu}(t) = \Delta\hat{e}\cdot\hat{\mu}(t), \tag{8}$$

defining the frequency fluctuation amplitude as $\Delta = \lambda E$. With angular free diffusion of the transition dipole being the sole source of spectral diffusion, the normalized frequency-frequency correlation functions obtained with the Stark model were[12]

$$R_{\text{para}}(t) = \frac{\langle\delta\omega(t)\,\delta\omega(0)\rangle_{\text{para}}}{\Delta^2/3} = \frac{3}{25}\left[\frac{11C_1(t)+4C_3(t)}{1+0.8C_2(t)}\right] \tag{9a}$$

for the $\langle XXXX\rangle$ case,

$$R_{\text{perp}}(t) = \frac{\langle\delta\omega(t)\,\delta\omega(0)\rangle_{\text{perp}}}{\Delta^2/3} = \frac{3}{25}\left[\frac{7C_1(t)-2C_3(t)}{1-0.4C_2(t)}\right] \tag{9b}$$

for the $\langle XXYY\rangle$ case, and

$$R_{\text{iso}}(t) = \langle\delta\omega(t)\,\delta\omega(0)\rangle\times 3/\Delta^2 = C_1(t) \tag{9c}$$

for the overall isotropic average. Here, $C_l(t) = \langle P_l(\hat{\mu}(t)\cdot\hat{\mu}(0))\rangle$ is the lth order Legendre polynomial orientational correlation function of the transition dipole unit vector.

To incorporate structural spectral diffusion into the previous results,[12] we now allow the field amplitude $E(t)$ and unit vector $\hat{e}(t)$ to be fluctuating quantities, which, in general, can be correlated. The vector frequency fluctuations are then given by Eq. (3), where the t dependence in θ_F is both due to the molecular probe transition dipole reorientation and the internal field directional fluctuations. The total frequency fluctuations also include electric field amplitude fluctuations. Therefore, the vector FFCF is

$$C_v^p(t) = \lambda^2\langle E(t)\,E(0)\cos(\theta_F(t))\cos(\theta_F(0))\rangle_p. \tag{10}$$

Following the original derivation of the $R_p(t)$ expressions in Eq. (9),[12] we begin from a frame in which $\hat{e}$ is directed along the z axis. In this "field frame," the transition dipole direction is specified by the coordinates $\hat{\mu}(t)\equiv\Omega_F(t) = (\theta_F(t),\phi_F(t))$ and hence,

$$\cos(\theta_F(t)) = \sqrt{\frac{4\pi}{3}}Y_1^0(\Omega_F(t)). \tag{11}$$

The orientation of the field frame relative to the lab frame is specified by the Euler angles $(\alpha_0, \beta_0, \gamma_0)$ at time zero and $(\alpha_1, \beta_1, \gamma_1)$ at time t. At time zero, suppose the orientation of the transition dipole in the lab frame is Ω_0. Then,

$$\cos\left(\theta_F\left(0\right)\right) = \sqrt{\frac{4\pi}{3}} \sum_m D^1_{m0}\left(\alpha_0, \beta_0, \gamma_0\right) Y^m_1\left(\Omega_0\right), \tag{12}$$

with D^l_{mn} a rotation matrix.[25] An analogous equation holds at time t, with dipole orientation Ω_1 in the lab frame. Returning to Eq. (10), we find

$$\begin{aligned}
\left\langle E\left(t\right) E\left(0\right) \cos\left(\theta_F\left(t\right)\right) \cos\left(\theta_F\left(0\right)\right)\right\rangle_p &= \frac{4\pi}{3}\left\langle E\left(t\right) E\left(0\right) \sum_{n,m} D^1_{n0}\left(\alpha_0, \beta_0, \gamma_0\right) Y^n_1\left(\Omega_0\right) D^1_{m0}\left(\alpha_1, \beta_1, \gamma_1\right) Y^m_1\left(\Omega_1\right)\right\rangle_p \\
&= \frac{4\pi}{3} \sum_{n,m} \left\langle E\left(t\right) D^1_{m0}\left(\alpha_1, \beta_1, \gamma_1\right) E\left(0\right) D^1_{n0}\left(\alpha_0, \beta_0, \gamma_0\right)\right\rangle \left\langle Y^m_1\left(\Omega_1\right) Y^n_1\left(\Omega_0\right)\right\rangle_p \\
&= \frac{4\pi}{3} \sum_{m} \left\langle E\left(t\right) D^1_{m0}\left(\alpha_1, \beta_1, \gamma_1\right) E\left(0\right) D^1_{-m0}\left(\alpha_0, \beta_0, \gamma_0\right)\right\rangle \left\langle Y^m_1\left(\Omega_1\right) Y^{-m}_1\left(\Omega_0\right)\right\rangle_p \\
&= \frac{4\pi}{3} \sum_{m} \left\langle E\left(t\right) D^1_{m0}\left(\alpha_1, \beta_1, \gamma_1\right) E\left(0\right) {D^1_{m0}}^*\left(\alpha_0, \beta_0, \gamma_0\right)\right\rangle \left\langle Y^m_1\left(\Omega_1\right) Y^{m*}_1\left(\Omega_0\right)\right\rangle_p,
\end{aligned} \tag{13}$$

making use of Eq. (A1) from Appendix A.

The electric field amplitude and direction correlation function appearing in Eq. (13) is an isotropic average because the vibrational transition dipole does not appear. Because every axis system is equivalent in an isotropic medium, the correlation function is independent of m.[26] This material correlation function can therefore be factored out of the sum, giving us

$$\begin{aligned}
\left\langle E\left(t\right) E\left(0\right) \cos\left(\theta_F\left(t\right)\right) \cos\left(\theta_F\left(0\right)\right)\right\rangle_p &= \left\langle E\left(t\right) D^1_{m0}\left(\alpha_1, \beta_1, \gamma_1\right) E\left(0\right) {D^1_{m0}}^*\left(\alpha_0, \beta_0, \gamma_0\right)\right\rangle \frac{4\pi}{3} \sum_m \left\langle Y^m_1\left(\Omega_1\right) Y^{m*}_1\left(\Omega_0\right)\right\rangle_p \\
&= \left\langle E\left(t\right) D^1_{m0}\left(\alpha_1, \beta_1, \gamma_1\right) E\left(0\right) {D^1_{m0}}^*\left(\alpha_0, \beta_0, \gamma_0\right)\right\rangle \times R_p\left(t\right).
\end{aligned} \tag{14}$$

The sum of polarization weighted spherical harmonic averages is precisely an intermediate expression which appeared in the calculation of the R_p factors in Eq. (9) originally.[12] We define the structural spectral diffusion vector coupling modulation as

$$F\left(t\right) = \lambda^2 \left\langle E\left(t\right) D^1_{m0}\left(\alpha_1, \beta_1, \gamma_1\right) E\left(0\right) {D^1_{m0}}^*\left(\alpha_0, \beta_0, \gamma_0\right)\right\rangle. \tag{15}$$

From Eqs. (10), (14), and (15), the vector PW-FFCF is thus the product of an isotropic SSD factor and a polarization-dependent RISD factor,

$$C^p_v\left(t\right) = F\left(t\right) R_p\left(t\right). \tag{16}$$

Note that the decays of both $F\left(t\right)$ and $C_s\left(t\right)$ may be referred to as structural spectral diffusion, because both functions decay due to structural fluctuations with rates independent of polarization. Where confusion may arise, these can be referred to as the vector modulation SSD and scalar SSD, respectively.

III. DECOMPOSITION OF THE FFCF FOR MODEL SYSTEMS

The analysis of 2D IR spectral diffusion data often focuses on inferring the dynamics of structural fluctuations from the FFCF. In the vector coupling case, it is the SSD factor F that reports on these dynamics. In this section, we examine the possible forms of the vector PW-FFCF by constructing several models of the structural modulation, Eq. (15), and the RISD correlation functions, Eq. (9).

A. Diffusive reorientation

In the simplest case, the orientational motion of the transition dipole can be taken to be diffusive. For this case, as treated previously,[12] the lth order Legendre polynomial orientational correlation function is

$$C_l\left(t\right) = \exp\left(-l\left(l+1\right) D_m t\right), \tag{17}$$

where D_m is the orientational diffusion constant. Then, the orientational correlation functions appearing in Eqs. (9) are simple exponentials. However, aside from the special case of isotropic weighting, (9c), the overall RISD correlation functions R_p themselves are, in general, non-exponential.

To examine the effects of structural spectral diffusion and reorientation-induced spectral diffusion operating simultaneously, we consider a normalized frequency-frequency correlation function of form (16). The inhomogeneous broadening is due to a vector interaction which can be modified both by structural changes (decay of $F\left(t\right)$) and transition dipole reorientation (decay of $R_p\left(t\right)$) to cause spectral diffusion. We model the SSD factor by the biexponential decay

$$F\left(t\right) = A_1 \exp\left(-t/\tau_1\right) + A_2 \exp\left(-t/\tau_2\right). \tag{18}$$

The strength and directionality of the strong vector interaction between the dipole and its surroundings lose correlation with increasing waiting time on two characteristic times, τ_1 and τ_2.

We let the second order orientational correlation time, which would be measured in a polarization-selective pump-probe (PP) experiment,[10,12,27–29] be fixed at $\tau_m = 1/\left(6D_m\right)$

TABLE I. FFCF structural spectral diffusion (A_i, τ_i) parameters. The biexponential fit (B_i, t_i) parameters that would be obtained when the effects of freely diffusive reorientation are included (data in Fig. 2).[a]

Case	A_1	τ_1 (ps)	A_2	τ_2 (ps)	Expt. type[b]	B_1	t_1	B_2	t_2
A	0.5	5	0.5	2000	∥	0.50	4.55	0.50	114.0
					⊥	0.51	4.96	0.49	75.3
B	0.5	5	0.5	150	∥	0.50	4.61	0.50	67.6
					⊥	0.51	4.91	0.49	51.2
C	0.5	5	0.5	50	∥	0.51	4.69	0.49	35.9
					⊥	0.50	4.84	0.49	30.2
D	0.5	5	0.5	20	∥	0.51	4.75	0.49	17.4
					⊥	0.50	4.79	0.50	15.8

[a]The free diffusion time constant (second order) is $\tau_m = 1/(6D_m) = 30$ ps.
[b]Fitting results are given for the parallel (∥) and perpendicular (⊥) experiments.

= 30 ps. The first SSD time constant, τ_1, will be fixed to be much faster than the reorientation rate at 5 ps. We will vary the second time τ_2 from much longer than the experimental window to just faster than the reorientation time. The parameters chosen for $F(t)$ in Eq. (18) are given in Table I. Decays of the polarization-weighted FFCF for a realistic waiting time range between zero and 100 ps were calculated using these parameters for both the $\langle XXXX \rangle$ (parallel) and $\langle XXYY \rangle$ (perpendicular) polarization configurations and are displayed in Figure 2 (points).

Though the RISD factors in Eq. (9) underlying the curves in Figure 2 are not multiexponential decays, the resulting products of structural and reorientational functions appear essentially indistinguishable from biexponential decays. If RISD influence (indicated by the faster decay of the perpendicular FFCF relative to parallel) was not anticipated by the experimenter, and only one of the data sets was obtained, typically $\langle XXXX \rangle$ (parallel), then analysis of this FFCF in terms of a biexponential decay would be the most straightforward approach. Biexponential fits to both data sets (parallel and perpendicular) appearing in Fig. 2 were performed and are displayed as solid lines. The agreement with the model data points is essentially perfect. The fit parameters (amplitudes, B_i, and time constants, t_i) are given in Table I.

For each case, A, B, C, and D, of structural spectral diffusion (the parameters are given in the left four columns of Table I), the results of the bi-exponential fits are given in the right four columns for both parallel and perpendicular experiments. In each case, a fast time constant t_1 between 4.5 and 5 ps and a slower time constant t_2, which depends strongly on the choice of τ_2, are observed. The amplitudes of both components, set to equal 0.5 in the biexponential SSD function in Eq. (18), are recovered almost without change caused by the RISD factor. Because the $\tau_1 = 5$ ps rate is several times faster than the reorientation rate, the fast SSD component is detected in both the parallel and perpendicular PW-FFCF decays almost unchanged. This is a key point — structural fluctuation rates sufficiently fast compared to any reorientation time scales are not accelerated by RISD in the observed FFCF and will appear almost identically in any polarization configuration.[12]

The slower component of the biexponential fit is where the majority of RISD's influence appears. The parallel and perpendicular R_p functions ((9a) and (9b)) decay somewhat slower and somewhat faster than $C_1(t)$ (9c), respectively, which decays at an easily determined rate of $3 \times \tau_m = 90$ ps. In Figure 2(a), in the absence of RISD, the 2 ns slow decay would appear as a constant offset (horizontal line). The offset would reflect structural inhomogeneity that appears static on the 100 ps maximum time scale we are considering because the experimental time range is limited by the vibrational lifetime. As can be seen in Table I, case A, the slower t_2 rate obtained from the fit is entirely due to the reorientation of the transition dipole sampling this very slowly evolving structural inhomogeneity. At intermediate rates of the slower SSD component,

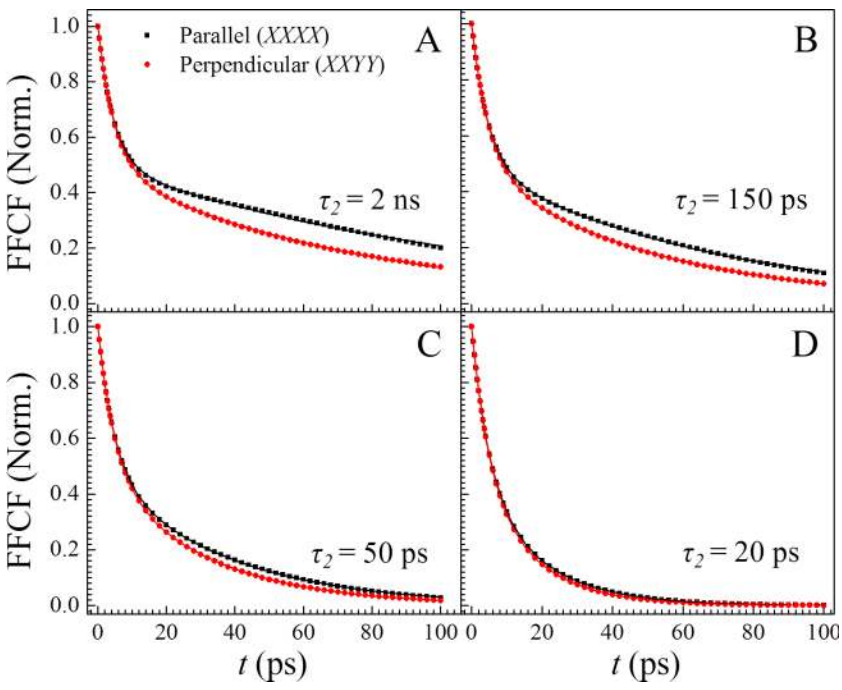

FIG. 2. Simulated parallel (black squares) and perpendicular (red circles) polarization-weighted FFCF data for various structural spectral diffusion rates, with a fixed orientational diffusion constant ($\tau_m = 30$ ps). (a) The slow time SSD ($\tau_2 = 2$ ns) is much slower than can be observed in the experimental window. RISD results in a significant difference in the parallel and perpendicular decays, which are greatly accelerated relative to the pure structural dynamics. For SSD time scales not substantially slower than the reorientation time (150 ps in (b) and 50 ps in (c)), the increase in decay rate and difference between polarization configurations is noticeable but lessened relative to (a). In (d), a SSD time of 20 ps (faster than τ_m) is nearly unaffected by the RISD contribution. Biexponential fits (solid lines) are displayed for each data set; the agreement with the data points is excellent.

as in Figs. 2(b) and 2(c), the rate constants for the structural fluctuations and frequency sampling due to reorientation (9) are combined to yield a slow component of the biexponential fit that is significantly faster than either contributing decay time (Table I). Finally, if the structural time scale is faster (even marginally) than the second order reorientation time (Fig. 2(d)), the addition of the RISD rate constant has a non-negligible but relatively small effect on the measured FFCF. For case D, the slow biexponential time scales given in Table I are a few picoseconds faster than the pure structural FFCF decay rate of 20 ps. Additionally, the parallel and perpendicular decays in Fig. 2(d) are barely discernible even in the absence of experimental noise. The coalescing of the $\langle XXXX \rangle$ and $\langle XXYY \rangle$ PW-FFCF decays corresponds well with the point at which the structural fluctuation time becomes faster than the reorientational time; therefore, the RISD has only a small effect.

For an analysis of experimental data, the CLS/FFCF from at least two polarization configurations should be obtained to confirm the presence or absence of reorientation-induced spectral diffusion on the observed decay. Suppose both the parallel and perpendicular PW-FFCFs have been determined. Under the assumption of free diffusion, the use of Eqs. (9), (16), and (18) implies 5 free parameters which can be determined simultaneously for both data sets. However, because of the complex form of RISD decay functions (9) and the versatility of multi-exponential decays in producing many decay shapes, it is likely that several combinations of structural decay rates/amplitudes and reorientation times could fit the data equally well.

To avoid such indeterminacies, the second order orientational correlation time can be directly determined from polarization-selective pump-probe experiments, which are frequently helpful in interpreting the spectral diffusion rates.[18] Therefore, the form of the RISD contribution can be independently constructed for any polarization configuration.[12] Determining SSD component (16), which is equal for all polarizations and modeled by a sum of exponentials, is then a much simpler task. A single polarization configuration can be fit with this model if the presence of RISD is already known. When more configurations are available, the single SSD function can be globally fit across all of the polarization-selective CLS/FFCF decays. These procedures will be illustrated through application to experimental CLS and anisotropy decays in Section IV.

Using this method, and assuming the reorientation time is independently known, the polarization-selective FFCF decays in Fig. 2 could be decomposed to recover the structural fluctuation time used in constructing the data sets. Recovering the longer structural time τ_2 from experimental data with these parameters would not be difficult for cases B, C, and D (Fig. 2 and Table I), because the structural part of the FFCF still contributes to the overall decay on the 100 ps time scale. The 2 ns decay of the SSD factor in case A could only be determined as an offset, i.e., an exponential term with effectively infinite time constant, because there is essentially no structural spectral diffusion caused by this term on the 100 ps time scale.

If the orientational relaxation (anisotropy decay) is measured with a pump-probe experiment and found to be a single exponential, there is a simple test to determine if RISD can be neglected. The pump-probe anisotropy decay is proportional to C_2, the second Legendre polynomial orientational correlation function.[30] RISD is dominated by C_1, the first Legendre polynomial orientational correlation function, which decays a factor of 3 times slower than C_2. If all of the decay components of the measured FFCF decay are fast compared to 3 times the second order orientational relation time from the pump-probe measurement, then RISD will make a negligible contribution to the FFCF. In this case, the measured FFCF directly yields the structural spectral diffusion dynamics.

B. Restricted orientational diffusion (wobbling-in-a-cone)

Frequently, orientational relaxation does not occur by free diffusion (single exponential decay for all orders of the orientational correlation function, Eq. (17)) because there are constraints on the regions of angular space that can be sampled by the vibrational probe molecule.[16,17,31] When orientational relaxation has time ranges in which restrictions prevent free diffusion, the orientational correlation function does not take the simple, single exponential, form of Eq. (17). However, for any (well determined) manner of orientational motion, the Legendre polynomial orientational correlation functions can still be calculated, and thus, Eqs. (9) remain applicable to describe the reorientation-induced contribution to spectral diffusion.[12]

Model-independent information appears in the orientational correlation functions in the form of a generalized order parameter, S_l.[17] In the long time limit, the lth order orientational correlation function will decay to the value S_l^2, assuming that both the absorption and emission transition dipole are parallel.[17] This is usually the case for vibrational transitions such as the hydroxyl stretch of methanol or the OH or OD stretch of HOD, for which the transition dipole is essentially the O–H or O–D bond.[21] The order parameter is defined by

$$S_l = \langle P_l(\cos\theta) \rangle = \int \mathrm{d}\Omega P_l(\cos\theta)\, p_{\mathrm{eq}}(\theta), \qquad (19)$$

with $p_{\mathrm{eq}}(\theta)$ the equilibrium probability distribution of transition dipole polar angles. The order parameter is intimately related to structural properties of the medium, i.e., how restricted the orientational motion is. The exact relationship between the order parameter and the structural information requires a model of the orientational motion. Furthermore, a model is necessary for any analysis of the time constant(s) of the orientational correlation decay.

A particularly straightforward model of restricted orientation relaxation is wobbling-in-a-cone.[16,17,31] In this model, the unique symmetry axis of the probe (i.e., the vibrational transition dipole direction) undergoes free diffusion within a cone of half angle θ_0. There is zero probability of finding the transition dipole direction outside of this cone. The order parameter within the wobbling-in-a-cone model is straightforward to calculate using Eq. (19) and the results for $l = 1$–4 are given in Table II.[17]

The exact time-dependent lth order orientational correlation function decays, however, are infinite sums of exponentials, with rate constants that cannot be obtained in closed form.[16,17,32] A simpler, single exponential, approximation to

TABLE II. Legendre polynomial orientational correlation function parameters for wobbling-in-a-cone dynamics.

l	$S_l = \langle P_l(\cos\theta)\rangle$[a]	$D_w\tau_{\text{eff}}^{(l)}\left(1-S_l^2\right)$[b]	$\tau_{\text{eff}}^{(l)}$ (small θ_0)[c]
1	$\frac{1+x_0}{2}$	$-\frac{(1+x_0)^2}{2(1-x_0)}\log[(1+x_0)/2]-\frac{x_0(4+x_0-x_0^2)}{4}$	$\frac{\theta_0^2}{D_w}\left(\frac{7}{24}-\frac{55\theta_0^2}{1152}\right)$
2	$\frac{x_0(1+x_0)}{2}$	$-\frac{x_0^2(1+x_0)^2(\log[(1+x_0)/2]+(1-x_0)/2)}{2(1-x_0)}$ $+\frac{(1-x_0)\left(6+8x_0-x_0^2-12x_0^3-7x_0^4\right)}{24}$	$\frac{\theta_0^2}{D_w}\left(\frac{7}{24}-\frac{35\theta_0^2}{384}\right)$
3	$\frac{(1+x_0)(5x_0^2-1)}{8}$	$-\frac{(1+x_0)^2(5x_0^2-1)^2\log[(1+x_0)/2]}{32(1-x_0)}$ $+\frac{30-9x_0+154x_0^2+231x_0^3-370x_0^4-615x_0^5+10x_0^6+185x_0^7}{384}$	$\frac{\theta_0^2}{D_w}\left(\frac{7}{24}-\frac{5\theta_0^2}{32}\right)$
4	$\frac{x_0(1+x_0)(7x_0^2-3)}{8}$	$-\frac{x_0^2(1+x_0)^2(7x_0^2-3)^2\log[(1+x_0)/2]}{32(1-x_0)}$ $+\frac{260+68x_0-1301x_0^2-1895x_0^3+6231x_0^4+9597x_0^5-7511x_0^6-13517x_0^7+497x_0^8+3731x_0^9}{3840}$	$\frac{\theta_0^2}{D_w}\left(\frac{7}{24}-\frac{35\theta_0^2}{144}\right)$

[a]Note that $x_0 = \cos\theta_0$, with θ_0 the hard-cone potential half angle.
[b]$l = 2$ result from Lipari and Szabo.[17]
[c]Limiting expressions for $\tau_{\text{eff}}^{(l)}$ apply at least up to $\theta_0 = 50°$ with less than 10% error (see Appendix B).

the orientational correlation function can be constructed as[17,32]

$$C_l(t) = S_l^2 + \left(1 - S_l^2\right)\exp\left(-t/\tau_{\text{eff}}^{(l)}\right). \tag{20}$$

Lipari and Szabo showed that the decay time constant $\tau_{\text{eff}}^{(l)}$ can be calculated, in closed form as a function of the cone angle θ_0 and diffusion constant D_w, such that the time integral of $C_l(t) - S_l^2$ is exact.[17] This integral defines the correlation time of either Eq. (20) or the complete orientational correlation function. As a result, Eq. (20) is an excellent approximation to the exact correlation function because it decays to the same offset with the same integrated time constant.

Lipari and Szabo originally derived $\tau_{\text{eff}}^{(2)}$ and S_2 to provide the second Legendre polynomial orientational correlation function.[17] This wobbling-in-a-cone orientational correlation function is extremely useful for the analysis of dipole reorientation observed in NMR Overhauser enhancement data,[17,33] fluorescence[17,31,32,34] and pump-probe[18,35,36] anisotropy decays, and time-domain optical heterodyne detected optical Kerr effect decays.[37–40] Our extension of the derivation is detailed in Appendix B, and the resulting expressions for $\tau_{\text{eff}}^{(l)}$ as a function of D_w and $x_0 = \cos\theta_0$ for l = 1–4 appear in Table II. As θ_0 approaches 180°, or $x_0 \to -1$, we find the appropriate limit $\tau_{\text{eff}}^{(l)} \to 1/(l(l+1)D_w)$ for free diffusion. Small angle approximations to $\tau_{\text{eff}}^{(l)}$, which are in error of less than 10% from the full expression for $\theta_0 < 50°$, are provided in Table II as well (see Appendix B).

Within the wobbling-in-a-cone model, therefore, the various Legendre polynomial orientational correlation functions can be directly related to one another. Once, for example, $C_2(t)$ is measured via the pump-probe anisotropy decay,[12,18] the wobbling-in-a-cone analysis yields θ_0 and D_w. Given these two constants, the order parameter and decay time constant are readily obtained for any other orientational correlation function (Table II). Thus, as in Section III A, measurement of $C_2(t)$ using polarization-selective pump-probe experiments allows the RISD contribution, in Eq. (9), to the overall spectral diffusion to be completely determined.

Within the first order Stark effect model considered so far, the orientational correlation functions for l = 1, 2, 3 are required (see Eq. (9)). Frequency fluctuations due to higher order Stark couplings are possible, in principle, and PW-FFCFs for these cases may be calculated using the same formalism detailed previously.[12] If a model related to the second order Stark effect is constructed, then $C_4(t)$ is required. For completeness, we have included the wobbling-in-a-cone order parameter and time constant for this correlation function in Table II.

A model is always necessary to relate a measured (or otherwise specified) orientational correlation function of a particular order to correlation functions of different orders. The two models discussed so far are free diffusion, as in Eq. (17), and the hard-cone formulation of the wobbling-in-a-cone model, as in Eq. (20). Other, possibly more realistic, models of restricted orientational motion have been discussed. One example is the harmonic cone model, which gives a Gaussian probability distribution of transition dipole orientations around a most probable direction.[31,41] Kinosita *et al.* showed that, particularly for smaller cone angles, the

hard-cone model and a harmonic cone with effective width equal to that of the hard-cone potential result in very similar correlation times for a given diffusion constant.[31] It appears that different models which capture the restriction of angular range (of the same magnitude) in some sense will yield similar correlation functions.[31] Therefore, even if the true orientational motion is not exactly described by the hard-cone model, we may still use this model to accurately relate orientational correlation functions of different orders.

The discussion so far assumes the wobbling anisotropy decay is well characterized by a single exponential to an offset, indicating relaxation within a single cone and no further orientational relaxation. In general, the observed anisotropy might be better described by a multi-exponential decay, indicating that there are multiple forms of independent reorientational motions. In this case, the total orientational correlation function can be regarded as the product of the correlation function for each independent contributor.[17,18,36] For instance, when a probe molecule is tethered to a much larger macromolecule, the probe's fast restricted wobbling motion is independent of the large particle's slow diffusive reorientational motion in the solvent. For such situations, Lipari and Szabo showed that the complete orientational correlation function obtained from the anisotropy decay ($l = 2$) is the biexponential function[17]

$$C_2(t) = \left(S_2^2 + \left(1 - S_2^2\right)\exp\left(-t/\tau_{\text{eff}}^{(2)}\right)\right)\exp\left(-t/\tau_m\right), \qquad (21)$$

with τ_m the overall diffusive reorientation time. Similarly, for any number of independent cones of restricted rotational motion,[18,36] and any overall slower rate of free diffusion, the total orientational correlation function of a particular order will be the product of one factor of Eq. (20) with appropriate order parameter and correlation time for each cone, and a factor of Eq. (17) for the final diffusive motion, which is the extension of Eq. (21) to multiple cones and arbitrary order.[18,36]

Model data were constructed to illustrate the effect of wobbling-in-a-cone orientational relaxation on the observed $\langle XXXX\rangle$ and $\langle XXYY\rangle$ PW-FFCF decays in the same manner as in Section III A. We fix the structural spectral diffusion parameters in Eq. (18) at $A_1 = 0.6$, $A_2 = 0.4$, $\tau_1 = 10$ ps, and $\tau_2 = 200$ ps. A component of the orientational relaxation is free diffusion with time constant (second order) of $\tau_m = 80$ ps. The free diffusion component in the RISD functions in Eq. (9) will serve to considerably accelerate the slow structural dynamics, but will have very little effect on the shorter time scale dynamics occurring in 10 ps. Several combinations of wobbling-in-a-cone parameters were chosen for illustration, particularly for their effect on the observed short time scale dynamics. The cone half angle θ_0 is varied between relatively small, 15°, and moderate, 30°. Additionally, the wobbling correlation time τ_c (second order, as could be determined from the pump-probe anisotropy in Eq. (21)) is varied from equaling the fast structural time scale, 10 ps, to being considerably faster at 1 ps.

The model data are displayed in Figure 3 (points) and the parameters used for these plots are collected in Table III. For the smaller 15° cone angle (Figs. 3(a) and 3(b)), it is only immediately apparent that the long time scale decay is influenced by RISD. There is nearly no observable difference between the parallel and perpendicular PW-FFCFs for waiting times below 20 ps. The biexponential fits (solid lines) describe the data very well. For the slower wobbling motion, Fig. 3(a), the amplitudes and time constants (Table III) are almost the same as those that would occur for solely diffusive reorientation with an 80 ps time constant. As the wobbling motion becomes faster to $\tau_c = 1$ ps (Fig. 3(b)), the biexponential fit amplitudes still closely match the input parameters for the structural spectral diffusion, but the short time constants in the fits are mildly decreased (~10%) by the fast wobbling motion.

When the cone angle is increased to 30° (Figs. 3(c) and 3(d)), it becomes more evident that the observed short time

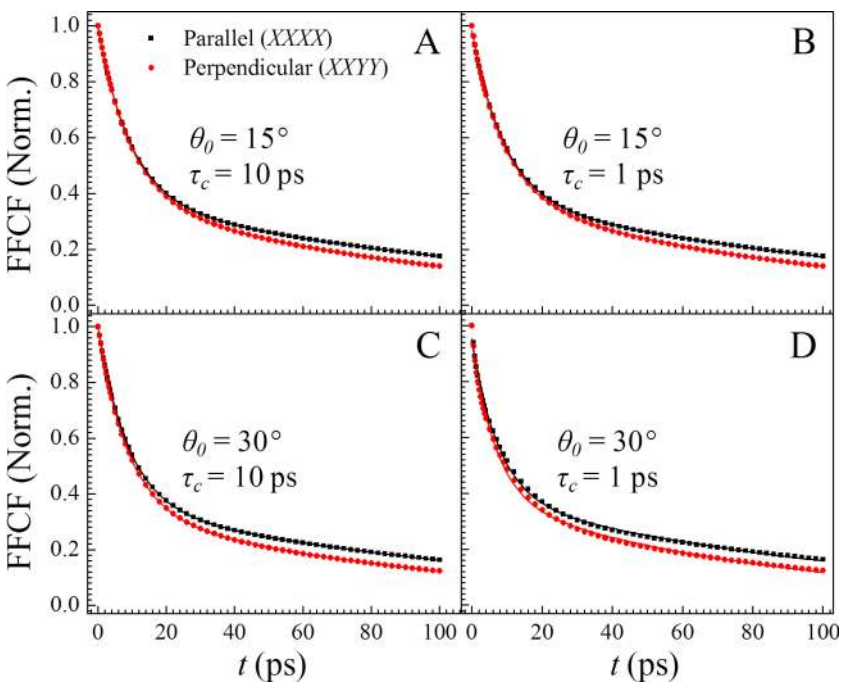

FIG. 3. Simulated parallel (black squares) and perpendicular (red circles) polarization-weighted FFCF data for fixed SSD parameters ($A_1 = 0.6$, $\tau_1 = 10$ ps, $A_2 = 0.4$, $\tau_2 = 200$ ps) and free diffusion time constant ($\tau_m = 80$ ps), with varying wobbling-in-a-cone half angles θ_0 and correlation times τ_c. The solid lines are biexponential fits. For smaller cone angles ((a) and (b)) and even relatively larger cones with slow orientational diffusion (c), the fits to the data points are essentially perfect. As the cone angle increases and the correlation time becomes short (d), biexponential decays show small discrepancies with the data at short to intermediate waiting times.

TABLE III. Free and restricted orientational diffusion (τ_m, τ_c, θ_0) parameters. The biexponential fit (B_i, t_i) parameters that would be obtained when the effects of the wobbling-in-a-cone reorientation are included (data in Fig. 3).[a]

Case	τ_m (ps)	θ_0 (deg.)	τ_c (ps)	Expt. type[b]	B_1	t_1 (ps)	B_2	t_2 (ps)
A	80	15	10	∥	0.62	9.45	0.38	128.6
				⊥	0.61	9.36	0.39	97.8
B	80	15	1	∥	0.60	9.13	0.39	124.5
				⊥	0.58	8.91	0.40	94.6
C	80	30	10	∥	0.64	8.86	0.36	125.2
				⊥	0.65	8.72	0.35	96.0
D	80	30	1	∥	0.56	7.52	0.39	111.2
				⊥	0.55	6.82	0.39	83.5

[a]The fast and slow structural correlation decay times are $\tau_1 = 10$ ps and $\tau_2 = 200$ ps, respectively, and the corresponding SSD amplitudes are $A_1 = 0.6$ and $A_2 = 0.4$.
[b]Fitting results are given for the parallel (∥) and perpendicular (⊥) experiments.

dynamics are influenced by RISD because there is a difference between the parallel and perpendicular decays on the 10-20 ps time scale. The effect is most noticeable for the faster correlation time of 1 ps in Fig. 3(d). For the longer wobbling correlation time of $\tau_c = 10$ ps (Fig. 3(c)), the biexponential fits still describe the model data points very well. The amplitudes are changed considerably, and the short time constant is sped up from the pure structural dynamics (Table III). Finally, for the shorter wobbling time constant of 1 ps (Fig. 3(d)), the curvature of the PW-FFCF decays at early times has increased to the point that biexponential fits can no longer capture the shape perfectly. The best fit curves for both $\langle XXXX \rangle$ and $\langle XXYY \rangle$ miss the points at both very short and intermediate time delays. In Table III, we observe that the short time amplitude is considerably decreased from the pure structural value (as opposed to the 10 ps case, which increased the amplitude) and both the long and short time constants are decreased substantially. Clearly, as the wobbling motion becomes both fast and larger in angular extent, the effect of RISD on the overall PW-FFCF decays increases to the point that multi-exponential fits no longer accurately yield the pure structural dynamics on the wobbling time scales.

C. Correlation time approach to wobbling dynamics

As in the free diffusion case considered in Section III A, the data constructed using a model containing both wobbling-in-a-cone and free diffusion dynamics, in Section III B, can be rigorously partitioned into their reorientation-induced and structural components. Given the wobbling parameters and free diffusion time from pump-probe measurements of $C_2(t)$, the correlation functions $C_1(t)$ and $C_3(t)$ and RISD factors R_p are readily constructed using Table II and Eqs. (9) to completely describe the RISD contribution. Fitting the data (either individually or globally over multiple polarization configurations) to the form of Eq. (16) is then straightforward.

In some cases, it may be desirable or necessary to describe the overall orientational correlation function in a simplified manner. For example, if wobbling dynamics and free diffusion contribute to the anisotropy decay as in Eq. (21) but the signal to noise ratio is not high enough to accurately resolve a biexponential decay (and fit the data as such), one would then describe the decay as a single exponential, corresponding to free diffusion as in Eq. (17). The correlation time is then a mixture of the wobbling and diffusive correlation times, with weighting between the two depending on the cone angle. We can integrate Eq. (21) to obtain the overall correlation time,

$$\tau_{\rm or} = \int_0^\infty C_2(t)\,{\rm d}t = \frac{1 - S_2^2}{1/\tau_{\rm eff}^{(2)} + 1/\tau_m} + S_2^2 \tau_m. \qquad (22)$$

The PW-FFCF data can be analyzed using this approximately diffusive correlation time to extract the structural spectral diffusion times and amplitudes with reasonable accuracy.

This method was applied to the PW-FFCF model data presented in Section III B. Orientational correlation functions of orders 1 and 3 were constructed using the overall correlation time with Eq. (17), and the parallel and perpendicular PW-FFCF data points were simultaneously fit including the biexponential SSD factor in Eq. (18). The results of the analysis are given in Table IV (labeling by case is the same as in Table III and Fig. 3). Representative fits using the single exponential orientational correlation approximation for fast wobbling dynamics ($\tau_c = 1$ ps) with both the small and medium sized cones followed by complete orientational randomization are shown in Figure 4. For slow wobbling dynamics, small cone angles, or both, the fitting results are in excellent agreement with the data points (small cone and fast dynamics case shown in the top panel of Fig. 4). In the case of $\theta_0 = 15°$ (cases A and B in Table IV), the extracted structural dynamics are acceptably close to the parameters used to construct the data (Table III). The amplitudes are recovered almost exactly and the short SSD time constant is less than 1 ps off from the true value of 10 ps.

As the cone angle increases to $\theta_0 = 30°$, the recovered SSD amplitudes have greater errors (cases C and D in Table IV). For the slower wobbling time (case C), the short structural time is recovered without large error, but the longer time dynamics are estimated as being considerably slower than the real value. In the case of both a moderate cone and fast wobbling dynamics (case D), the fit to the data points disagrees on the very short and intermediate time scales (Fig. 4, bottom). In this case, the extracted short time structural dynamics are much too rapid, though the long time dynamics were more correctly captured in the fit than in the case of a longer wobbling time scale (case C). Overall, larger cone angles are more detrimental to the quality of this analysis than faster correlation times, though both have a noticeable effect.

TABLE IV. Biexponential structural fluctuation (SSD) parameters (a_i, t_i) obtained in the wobbling case using the integrated orientational correlation time $\tau_{\rm or}$.[a]

Case	$\tau_{\rm or}$ (ps)	a_1[b]	t_1 (ps)	a_2[b]	t_2 (ps)
A	73.0	0.61	9.76 ± 0.02	0.39	212 ± 1
B	72.2	0.59	9.34 ± 0.08	0.40	202 ± 4
C	55.3	0.64	9.20 ± 0.09	0.36	275 ± 10
D	52.6	0.55	7.4 ± 0.2	0.40	217 ± 16

[a]Exact orientational correlation function parameters are given in Table III.
[b]Error in extracted amplitudes is at most on the order of 10^{-3}.

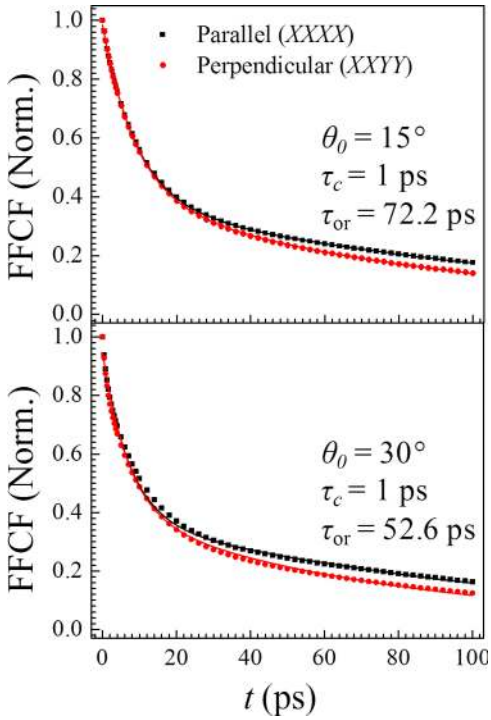

FIG. 4. Representative fits to the parallel and perpendicular PW-FFCFs generated with wobbling-in-a-cone reorientation dynamics (Figure 3 and Table III), assuming an average correlation time giving effective single exponential diffusive orientational motion. Top, smaller cone: 15°. Bottom, larger cone: 30°. Both have a wobbling time constant $\tau_c = 1$ ps, corresponding to (b) and (d) of Fig. 3. As the cone angle increases, the simplified model cannot accurately fit the two datasets except at long waiting times.

With relatively small cone half angles and slow wobbling dynamics, the fit results shown in Table IV and Fig. 4 are acceptable. When these limits can be argued for on physical grounds, the overall correlation time analysis detailed above can be safely applied. However, given detailed knowledge of the complete C_2 orientational correlation function, the full wobbling-in-a-cone analysis using Table II enables extraction of accurate structural spectral diffusion times and amplitudes for any combination of orientational diffusion parameters.

IV. ANALYSIS OF H-BONDED HYDROXYLS IN RTILs

A. Methanol in HmimPF$_6$

Polarization-selective CLS decay rates were previously reported for the hydroxyl (O–D) stretching mode of dilute methanol-d$_4$ (simply methanol henceforth) in the room temperature ionic liquid HmimPF$_6$ (structure shown in Figure 5).[12] Comparison of the parallel and perpendicular polarized CLS decays and the anisotropy decay, which was measured with pump-probe experiments, showed clearly that both reorientation-induced and structural spectral diffusions contribute to the frequency sampling of the inhomogeneously broadened absorption spectrum. The exact partitioning of the two effects can now be determined using the results in Sections II and III.

The PP anisotropy decay was shown previously at a single representative detection frequency, the peak of the PP spectrum

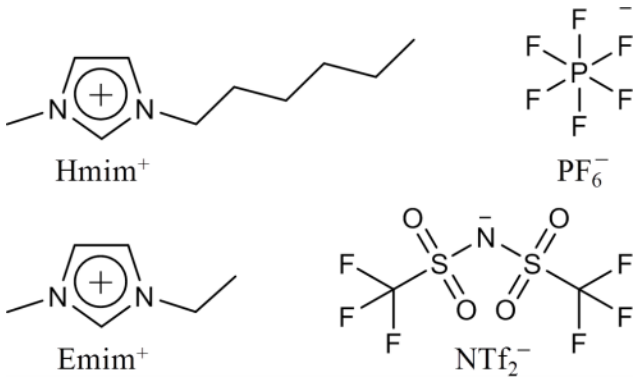

FIG. 5. Structures of the room temperature ionic liquids. 1-hexyl-3-methylimidazolium (Hmim$^+$) hexafluorophosphate (PF_6^-) (top), and 1-ethyl-3-methylimidazolium (Emim$^+$) bis(trifluoromethylsulfonyl)imide (NTf_2^-) (bottom).

at 2667 cm^{-1}.[12] Because methanol's hydroxyl stretch band has a FWHM of 23 cm^{-1} that is much smaller than the anharmonicity of about 90 cm^{-1}, the anisotropy can be analyzed across the entire 0-1 line shape. Six detection frequencies between 2646.8 and 2680.6 cm^{-1} span the 0-1 band, with high enough signal to noise ratio for reliable fitting. Similarly to the previous experiments on the hydroxyl stretch of dilute alcohols in RTILs,[18] the anisotropy decays at all frequencies were simultaneously fit to triexponential functions, with the amplitudes allowed to vary freely but the time constants constrained to be equal at all frequencies. Essentially, quantitative agreement with the data was found, similar to the fit displayed previously at 2667 cm^{-1}.[12]

The resulting triexponential fits were analyzed further in terms of the wobbling-in-a-cone model, with a single inertial cone, whose correlation time is too short to detect, two cones with observed diffusive wobbling dynamics, and a final period of free orientational diffusion that completely randomizes the orientations.[18] The cone angles are displayed in Figure 6(a). Each individual cone corresponds to an $l = 2$ order parameter (Table II). The product of these order parameters is the total order parameter for the restricted angular motion, and the cone angle corresponding to the total order parameter is that of the total cone, which captures the overall angular range which is sampled prior to free diffusion. The second order correlation times that emerge from the analysis are $\tau_{c1} = 1.0 \pm 0.4$ ps for the first cone, $\tau_{c2} = 9 \pm 2$ ps for the second cone, and a free diffusion time constant, $\tau_m = 101 \pm 13$ ps.

To fit the CLS decay data (Figure 6(b)), the cone angles and correlation times can be used to construct the $C_1(t)$ and $C_3(t)$ orientational correlation functions, in addition to the known $C_2(t)$. The present theory assumes frequency-independent reorientation dynamics. While the second order wobbling correlation times are indeed frequency-independent, there is some variation in the cone angles (Figure 6(a)) with frequency, because redder frequencies report on hydroxyls engaged in stronger hydrogen bonds, which more tightly restrict angular motion.[18,21,22] The CLS data were obtained from the 2D IR line shapes around the center of the band.[12] Therefore, the cone angles at the center frequency of the PP spectrum at 2667 cm^{-1} are used for the CLS analysis.

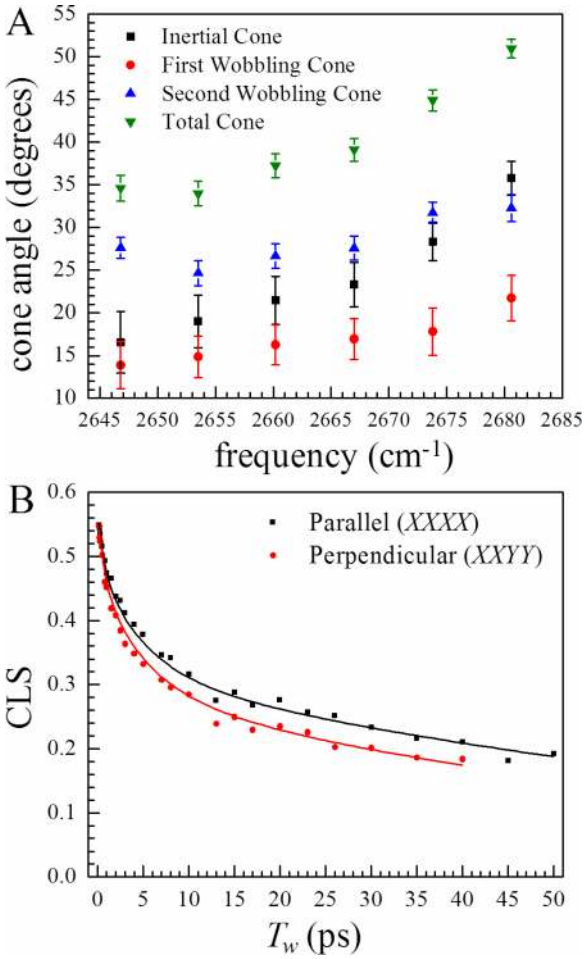

FIG. 6. Analysis of pump-probe anisotropy and polarization-selective CLS of the O–D stretch of methanol-d_4 in $HmimPF_6$. (a) Results of wobbling-in-a-cone analysis from global fit of the anisotropy decay. The total cone expresses the overall angular range in which the transition dipole is initially confined (see text). (b) Simultaneous fit (lines) to the parallel and perpendicular polarization configuration CLS data (points) with the RISD contribution fixed by the wobbling-in-a-cone decomposition of the measured anisotropy. The cone angles from line center (2667 cm^{-1}), which are most representative of the entire band, are used in this analysis.

Additionally, because the center of the band has the greatest population, the parameters obtained here, rather than at the edges, are most representative of the majority of methanol molecules contributing to the nonlinear signal. The values are $\theta_{in} = 23° \pm 3°$, $\theta_{c1} = 17° \pm 2°$, and $\theta_{c2} = 28° \pm 1°$ for the inertial, first wobbling, and second wobbling cone, respectively, at detection frequency 2667 cm^{-1} (Fig. 6(a)). Note that because the total cone angle is not small, assuming an average correlation time for orientational diffusion will not be appropriate (see Section III C and Fig. 4).

To extract the SSD part from the two CLS decays, we fit the parallel and perpendicular CLS data (Figure 6(b)) using Eq. (16), i.e., a product of a SSD factor $F(t)$ and a RISD factor $R_p(t)$. The polarization-dependent RISD factor $R_p(t)$ is fixed by the wobbling-in-a-cone analysis of the measured anisotropy (see Section III B), and the polarization-independent SSD factor $F(t)$ is obtained by simultaneously fitting both polarization-selective CLS decays. The solid lines in Figure 6(b) are from the triexponential SSD and RISD simultaneous fit. Fit curves for a biexponential model of the SSD appear quite similar, though the triexponential model describes the data somewhat better. Both biexponential and triexponential fitting parameters are listed in Table V (bottom portion). For comparison, the biexponential fits to the CLS decays in the $\langle XXXX \rangle$, $\langle XXYY \rangle$, and $\langle XYXY \rangle$ polarization configurations are included in Table V (top portion) as well.[12]

The fit curves using the SSD with RISD formalism are in excellent agreement with both CLS datasets in Figure 6(b) at short and long times. At intermediate waiting times, the fit underestimates the CLS slightly for parallel and overestimates similarly for perpendicular. The disagreement is minor, however, and overall the simultaneous fit gives a good description of both datasets over the entire experimentally accessible waiting time (T_w) range. The fitting results for $F(t)$, the structural spectral diffusion correlation function, are given in Table V. With the triexponential model, there is a small amplitude, very fast component with sub-picosecond duration which is expected for hydrogen bonded hydroxyls in ionic liquids,[18] an intermediate component with time constant 5 ps (slightly slower than the ~3 ps time constant in the $\langle XXXX \rangle$ and $\langle XXYY \rangle$ biexponential fits), and a much larger and slower component than the final decay of the direct biexponential fits (Table V).[12]

In a previous publication, in addition to the parallel and perpendicular polarization configurations discussed in depth in this paper, 2D IR spectra were acquired with the "polarization grating" configuration, $\langle XYXY \rangle$. The polarization grating configuration CLS decay rate was much slower than the other

TABLE V. Results of direct CLS fits and structural spectral diffusion (SSD) parameters obtained when RISD is properly included for methanol-d_4 in $HmimPF_6$.

Experiment/fit type	A_1	τ_1 (ps)	A_2	τ_2 (ps)	A_3	τ_3 (ps)
Direct CLS fits[a]						
$\langle XXYY \rangle$	...	...	0.23 ± 0.01	2.2 ± 0.4	0.32 ± 0.01	63 ± 6
$\langle XXXX \rangle$	...	...	0.20 ± 0.01	3.2 ± 0.4	0.34 ± 0.01	76 ± 7
$\langle XYXY \rangle$	...	...	0.14 ± 0.01	3.3 ± 0.6	0.41 ± 0.01	149 ± 19
SSD with RISD results from global fits						
Biexponential SSD	...	...	0.19 ± 0.01	2.7 ± 0.3	0.41 ± 0.01	98 ± 9
Triexponential SSD	0.07 ± 0.02	0.6 ± 0.3	0.16 ± 0.02	5 ± 1	0.38 ± 0.02	119 ± 20

[a]Values reported previously as complete FFCFs.[12] CLS fit results here are for the normalized T_w-dependent part of the total FFCF.[3,4]

two configurations. The slow decay time constant obtained from the $\langle XYXY \rangle$ polarization CLS, 149 ± 19 ps,[12] interestingly agrees well (the error bars overlap) with the slowest triexponential time constant of the SSD component, 119 ± 20 ps, which we extracted from the parallel and perpendicular polarization configurations here (see Table V). The ratio of the slow component amplitude to the fast component amplitude for the $\langle XYXY \rangle$ CLS, $A_3/A_2 = 2.9$, is also most similar to $A_3/A_2 = 2.4$ for the triexponential model obtained here for SSD component. It appears that the CLS decay in the $\langle XYXY \rangle$ configuration gives the best estimate of the pure structural spectral diffusion contribution to the overall spectral diffusion, as obtained from the analysis explicitly treating the RISD contribution.

The biexponential SSD model (Table V) allows us to more easily examine the effects of reorientation-induced spectral diffusion on the amplitudes of structural dynamics that were originally determined from the data (direct CLS biexponential fits at the top of Table V). The short time constant extracted using the full RISD analysis does not differ from that obtained by straightforward biexponential fits of the CLS data.[12] However, the relative amplitude of the slower component to the faster one is underestimated in the simple biexponential fits for the $\langle XXXX \rangle$ and $\langle XXYY \rangle$ configurations. Furthermore, the slower time constant (around 70 ps for parallel or perpendicular[12]) is underestimated from 119 ps in the SSD and RISD analysis as well (see Table V). These observations are precisely what is anticipated based on the model calculations presented in Section III.

As discussed in Section II, an additive FFCF term, which is independent of the polarization configuration being considered, can possibly exist if there are frequency fluctuations that do not originate from vector interactions. The experimental results on methanol in $HmimPF_6$ discussed above are readily analyzed without inclusion of such a term; thus, we believe that for this system such an additive term's contribution is minor.

One situation (yet to be observed in experimental spectral diffusion data) in which an additive term may be clearly required is if two different polarization-selective CLS curves converge to the same final decay, which begins considerably above a CLS value of zero. It is typically the slowest structural dynamics (which couple as a vector to the transition dipole) that will be most perturbed by RISD. Therefore, the greatest difference between two polarization configurations, parallel and perpendicular, will occur on this longest time scale. It is evident from the model curves presented with the original theory of RISD[12] and in Figure 2, with the inclusion of SSD, that the parallel and perpendicular PW-FFCF decays only become equal as they approach zero frequency correlation. If the polarization-selective CLS decays converge before this point, then accurate fitting of the two (or more) decays may require a polarization-independent additive term that should be simultaneously fit for all configurations.

With the structural part of the (normalized) vector FFCF having been determined from the data (Table V), in principle, the polarization-weighted FFCF or CLS decay for any $\langle AABB \rangle$ polarization configuration can be calculated using Eqs. (9) or similar ones derived within the same formalism.[12] One situation in which this may be useful is in comparison to MD simulations. Often the 2D IR experiments are done in the $\langle XXXX \rangle$ configuration, but the FFCF calculated directly from a MD trajectory is isotropically averaged.[20–22] Once the SSD factor $F(t)$ is obtained, it is straightforward to calculate the isotropically averaged FFCF using Eqs. (16) and (9c).

B. Water, methanol, and ethanol in $EmimNTf_2$

Prior to investigations of reorientation-induced spectral diffusion in 2D IR spectroscopy, the structural and orientational dynamics of dilute water (partially deuterated to HOD), methanol-d_4, and ethanol-d_6 in the RTIL $EmimNTf_2$ (Fig. 5) were examined with 2D IR and polarization-selective pump-probe spectroscopy, respectively.[18] Only the $\langle XXXX \rangle$ CLS was obtained because this is the standard configuration which maximizes the nonlinear signal.[30] The orientational dynamics were readily analyzed using the wobbling-in-a-cone model, so we may construct the orientational correlation functions for $l = 1$ and $l = 3$ to perform a similar analysis to that in Section IV B for the RTIL $HmimPF_6$. Because RISD had a considerable effect on an alcohol in a different ionic liquid, it is possible that these data contain RISD influence as well.

Orientational correlation function parameters (i.e., cone angles) corresponding to the peak frequency of the PP spectrum were used for each vibrational probe. The CLS data were originally described extremely well by triexponential decays.[18] We re-fit the data using Eq. (16) with the RISD contribution for $\langle XXXX \rangle$ configuration fixed by the known orientational correlation functions and a triexponential model for the structural dynamics. The resulting short and intermediate SSD time constants were equal to the triexponential CLS fit values within the error bars. The amplitude for the longest time scale structural dynamics was found to be somewhat larger than would be inferred from the direct CLS fit. In this case, the effect of RISD was to reduce the amplitude observed for the slowest component by between 10% and 15%. While the amplitude of the slowest frequency fluctuations is underestimated, it is a relatively minor effect.

The most noticeable difference, however, is in the slowest spectral diffusion time constant. While the times from the direct CLS fit with no consideration of RISD were 23 ± 3 ps, 28 ± 1 ps, and 34 ± 3 ps for water, methanol, and ethanol, respectively,[18] the time constants for the slowest SSD component extracted from the SSD and RISD fit are 30 ± 5 ps, 33 ± 2 ps, and 37 ± 3 ps. While the decay times for the slowest component have become somewhat slower, the trend is the same. There is still a mild slowing of this time constant with alkyl chain length, although these three values have overlapping error bars. For alcohols in the $EmimNTf_2$ system, it appears that the overall effect of RISD is much less dramatic than in the $HmimPF_6$ system.

$EmimNTf_2$ is much less viscous than $HmimPF_6$; the room-temperature viscosities are 31 cP and 497 cP, respectively.[42,43] For all the water/alcohol probes in $EmimNTf_2$, the slowest SSD component is much faster than for methanol in $HmimPF_6$. Considering water, methanol, and ethanol, respectively, in $EmimNTf_2$, the slowest components of orientational relaxation (by free diffusion) measured by the PP anisotropy were 25.1 ± 0.7 ps, 42 ± 1 ps, and 88 ± 10 ps.[18] The corresponding ratios

of these reorientation times to the slowest SSD relaxation time scales (above) are 0.84, 1.3, and 2.4. For methanol in $HmimPF_6$, the ratio of the slowest orientational to the slowest SSD time is 0.84. With the larger methanol and ethanol probes in $EmimNTf_2$, the reorientation time is longer than the structural fluctuation time scale, unlike for methanol in $HmimPF_6$. The result is that RISD has a non-negligible influence on the experimentally determined structural spectral diffusion dynamics, but the RISD corrected values have overlapping error bars with direct fit values.

Water exhibits particularly fast orientational motions in $EmimNTf_2$, and similarly to methanol in $HmimPF_6$, there was a significant acceleration of the long time scale spectral diffusion by RISD. As the probe size is increased, to methanol and ethanol, this RISD effect becomes progressively smaller due to the slowing of the reorientation dynamics.[18] The relatively large acceleration of water's slowest structural spectral diffusion rate through RISD is 23%. For the $\langle XXXX \rangle$ configuration, a multi-exponential fit for methanol in $HmimPF_6$ gives a slowest decay constant that is faster by 36% relative to the true SSD rate obtained using the full analysis including RISD (Table V).

V. CONCLUDING REMARKS

By considering electric fields internal to the sample which can evolve both in amplitude and direction, independently of the reorientation of the vibrational probe molecule, the first order Stark effect model of reorientation-induced spectral diffusion[12] was successfully extended to include the effects of structural spectral diffusion. To further capture the complex dynamics expected in real condensed phase systems, restricted orientational motion of the vibrational probe's transition dipole was addressed using the wobbling-in-a-cone model. Within this model, the orientational correlation function measured using the pump-probe anisotropy decay, $C_2(t)$, directly yields the other orientational correlation functions, $C_1(t)$ and $C_3(t)$, necessary for calculating RISD's influence on the polarization-weighted FFCF.

Through model calculations using biexponential SSD dynamics, we found that simple biexponential decay fits to the parallel or perpendicular configuration CLS cease to accurately extract the structural dynamics of the medium and instead are substantially influenced by reorientation of the vibrational transition dipole, as the reorientation dynamics become faster. In particular, fast orientational dynamics means that $3 \times \tau_m$, the characteristic time scale of the first order orientational correlation function, is less than or comparable to the structural spectral diffusion time scale of interest. In the restricted angular diffusion case, small cone angles and longer correlation times influenced the faster components of structural spectral diffusion relatively little. In these cases, treating the overall reorientation dynamics as diffusive using a single correlation time within the RISD model was acceptable. When the cone angles become large and the wobbling becomes fast, however, the orientational correlation functions must explicitly include the wobbling dynamics to adequately separate the SSD and RISD contributions to the polarization-selective CLS decays.

The complete wobbling-in-a-cone formalism allowed us to use the measured anisotropy decays to fit the CLS including SSD and RISD for alcohol probes in two ionic liquid systems, $HmimPF_6$ and $EmimNTf_2$.[12,18] For the $HmimPF_6$ system, the slow component amplitude and time obtained from fitting the CLS directly with a biexponential decay were found to be considerably smaller and shorter, respectively, than the true structural spectral diffusion FFCF decay. Only by fitting with inclusion of the RISD factor could the actual SSD time constants be obtained without significant error. For the $EmimNTf_2$ system, a more mild slowing of the slowest structural spectral diffusion time constants was found for the water, methanol, and ethanol solutes, compared to the values originally reported, but the trend was the same. The longest time component of the SSD dynamics progressively slows as the size of the probe molecule increases.

When can RISD be neglected? First, if the orientational relaxation measured by a pump-probe experiment is slow compared to all time scales of the 2D IR measured FFCF, RISD will not influence the observed decay. As a rule of thumb, if three times the orientational relaxation time is large compared to the slowest component of the measured FFCF, RISD analysis is unnecessary. If the orientational relaxation contains wobbling-in-a-cone dynamics, but the cone angles are small and the final complete orientational relaxation time is slow as discussed above, only a small error in the fast SSD decay times and amplitudes will be introduced by neglect of RISD. If orientational relaxation is not slow compared to the measured 2D IR FFCF decay, but the FFCFs of two clearly distinct polarization configurations such as $\langle XXXX \rangle$ and $\langle XXYY \rangle$ are the same, then RISD is not playing a role in the spectral diffusion. That is, the coupling of the vibrational transition to its surroundings is a scalar, not a vector, and the experimentally determined FFCF gives the pure structural dynamics.

Finally, it is important to discuss situations in which vibrational probe reorientation contributes to spectral diffusion but is not RISD. Water is a useful example. There is a key difference between the correlation of orientational and spectral fluctuations that is well-established for the bulk water system (HOD in H_2O or D_2O), and the strong vector dependence of the frequency fluctuation on probe orientation observed in recent experiments on methanol in the RTIL $HmimPF_6$.[12] Methanol reorientation in the ionic liquid occurs without complete randomization of the liquid structure. On methanol orientational time scales, a component of the structure that contributes to the overall inhomogeneous broadening of the absorption line shape can, therefore, be considered static. Spectral diffusion is, to a large degree, the result of the time evolution of the probe's interaction with this slow structural component through the transition dipole's angular motions. The structure itself changes only on longer time scales. Reorientation of methanol in $HmimPF_6$ does not change all the aspects of the liquid structure; only the coupling of the methanol by a vector interaction with this structure is modified by reorientation.

The situation in the methanol/$HmimPF_6$ system is very different from bulk water.[12] No component of the structure in bulk water is slow on the time scale of reorientation because

reorientation is a major component of the structural reorganization mechanism.[8,9,22,23,35] The hydroxyl (O–D stretch of HOD or O–H of HOD) interacts through hydrogen bonds with its surroundings. Rearrangement of the hydrogen bonding network involves reorientation of the water molecules, so reorientation is involved in changes of the vibrational frequency. However, the structure is evolving fast enough through structural changes, including reorientation of other water molecules, that only structural spectral diffusion determines the overall FFCF decay. Therefore, RISD can be ignored for bulk water, because reorientation (three times the orientational relaxation rate) is slow on structural evolution time scales.

ACKNOWLEDGMENTS

We thank Chiara Giammanco and Amr Tamimi for helpful discussions and comments on the manuscript. This work was funded by the Division of Chemical Sciences, Geosciences, and Biosciences, Office of Basic Energy Sciences of the U.S. Department of Energy through Grant No. DE-FG03-84ER13251 (P.L.K. and M.D.F.), and the Air Force Office of Scientific Research Grant No. FA9550-12-1-0050 (J.N. and M.D.F.). P.L.K. and J.N. acknowledge support from Stanford Graduate Fellowships.

APPENDIX A: DERIVATION OF ROTATION MATRIX ORTHOGONALITY WITH AMPLITUDE FACTORS IN CORRELATION FUNCTION AVERAGES

We derive the result

$$\left\langle E_1 D^l_{nm}(\alpha_1,\beta_1,\gamma_1)\, E_0 D^k_{n'm'}(\alpha_0,\beta_0,\gamma_0)\right\rangle \propto \delta_{n,-n'}\delta_{m,-m'}, \quad \text{(A1)}$$

which was used in Section II to separate the vector FFCF into SSD and RISD factors. This derivation is closely related to the one used by Nishida and Fayer to show that the spherical harmonics $Y^m_2(\theta,\phi)$ are orthogonal with respect to m inside of correlation function averages, even in uniaxial systems.[44] The generality of the proof is useful in the present investigation because we do not need to make any assumptions about the correlation between the amplitude and orientational factors.

To begin, we recall

$$D^l_{nm}(\alpha,\beta,\gamma) = e^{-in\alpha} d^l_{nm}(\beta)\, e^{-im\gamma}, \quad \text{(A2)}$$

where d^l_{nm} is Wigner's small d-matrix.[25] The Euler angles and amplitudes, respectively, evolve from $\Omega_0 = (\alpha_0,\beta_0,\gamma_0)$ and E_0 at time zero to $\Omega_1 = (\alpha_1,\beta_1,\gamma_1)$ and E_1 at time t according to the probability evolution Green's function, $G(t;\Omega_1,\Omega_0,E_1,E_0)$. In an isotropic system, the initial probability distribution is $P(\Omega_0) = 1/8\pi^2$. The amplitude initial probability distribution is given by $P(E_0)$. The correlation function average can be written as

$$\begin{aligned}
&\left\langle E_1 D^l_{nm}(\alpha_1,\beta_1,\gamma_1)\, E_0 D^k_{n'm'}(\alpha_0,\beta_0,\gamma_0)\right\rangle \\
&\quad = \int \mathrm{d}\Omega_1 \int \mathrm{d}\Omega_0 \int \mathrm{d}E_1 \int \mathrm{d}E_0 E_1 D^l_{nm}(\Omega_1)\, G(t;\Omega_1,\Omega_0,E_1,E_0)\, E_0 D^k_{n'm'}(\Omega_0)\, P(E_0)\, P(\Omega_0) \\
&\quad = \frac{1}{8\pi^2}\int_0^\pi \sin\beta_1 \mathrm{d}\beta_1 \int_0^\pi \sin\beta_0 \mathrm{d}\beta_0 d^l_{nm}(\beta_1)\, d^k_{n'm'}(\beta_0) \int_{-\infty}^{\infty}\mathrm{d}E_1 \int_{-\infty}^{\infty}\mathrm{d}E_0 P(E_0)\, E_1 E_0 \\
&\qquad \times \int_0^{2\pi}\mathrm{d}\alpha_1 \int_0^{2\pi}\mathrm{d}\alpha_0 \int_0^{2\pi}\mathrm{d}\gamma_1 \int_0^{2\pi}\mathrm{d}\gamma_0 e^{-in\alpha_1} e^{-im\gamma_1} e^{-in'\alpha_0} e^{-im'\gamma_0} G(t;\Omega_1,\Omega_0,E_1,E_0)\,.
\end{aligned} \quad \text{(A3)}$$

In the final expression, the second factor, referred to as I, contains an integral over the α and γ angles, which depends on n, n', m, and m'. The I part will give us the orthogonality properties we seek to prove. The variables β_1, β_0, E_1, and E_0 are held constant in evaluating the four integrals contained in this factor.

We have assumed the system is isotropic, so only the differences $\alpha_1 - \alpha_0$ and $\gamma_1 - \gamma_0$ are relevant in the Green's function. The remaining parameters are summarized by $\Theta = (\beta_1,\beta_0,E_1,E_0,t)$ and do not affect the I integral values. We may then cast the Green's function in the form

$$G(t;\Omega_1,\Omega_0,E_1,E_0) = g_\Theta(\alpha_1-\alpha_0,\gamma_1-\gamma_0) \quad \text{(A4)}$$

noting that $g_\Theta(\phi,\chi)$ is 2π-periodic in both ϕ and χ.[44] Define

$$h_{\Theta,n',m'}(\alpha_1-\alpha_0,\gamma_1-\gamma_0) = e^{in'(\alpha_1-\alpha_0)+im'(\gamma_1-\gamma_0)} g_\Theta(\alpha_1-\alpha_0,\gamma_1-\gamma_0)\,; \quad \text{(A5)}$$

clearly, $h_\Theta(\phi,\chi)$ maintains the periodicity of g_Θ. We may then write

$$\begin{aligned}
I &= \int \mathrm{d}(\alpha_1,\alpha_0,\gamma_1,\gamma_0)\, e^{-in\alpha_1} e^{-im\gamma_1} e^{-in'\alpha_0} e^{-im'\gamma_0} g_\Theta(\alpha_1-\alpha_0,\gamma_1-\gamma_0) \\
&= \int \mathrm{d}(\alpha_1,\alpha_0,\gamma_1,\gamma_0)\, e^{-i(n+n')\alpha_1} e^{-i(m+m')\gamma_1} h_{\Theta,n',m'}(\alpha_1-\alpha_0,\gamma_1-\gamma_0)\,,
\end{aligned} \quad \text{(A6)}$$

where the integration variables and limits have been abbreviated from (A3). Observe that $h_{\Theta,n',m'}$ can be expanded in a two-dimensional Fourier series, because of its 2π-periodicity,

$$h_{\Theta,n',m'}(\phi,\chi) = \sum_{r,s} c^{\Theta,n',m'}_{rs} e^{-ir\phi} e^{-is\chi}. \quad \text{(A7)}$$

We may now evaluate I using this expansion as follows:

$$\begin{aligned} I &= \sum_{r,s} c_{rs}^{\Theta,n',m'} \int \mathrm{d}\left(\alpha_1,\alpha_0,\gamma_1,\gamma_0\right) e^{-i(n+n')\alpha_1} e^{-i(m+m')\gamma_1} e^{-ir(\alpha_1-\alpha_0)} e^{-is(\gamma_1-\gamma_0)} \\ &= \sum_{r,s} c_{rs}^{\Theta,n',m'} \int \mathrm{d}\left(\alpha_0,\gamma_0\right) e^{-ir\alpha_0} e^{-is\gamma_0} \int \mathrm{d}\left(\alpha_1,\gamma_1\right) e^{-i(n+n'-r)\alpha_1} e^{-i(m+m'-s)\gamma_1} \\ &= 4\pi^2 c_{00}^{\Theta,n',m'} \int \mathrm{d}\left(\alpha_1,\gamma_1\right) e^{-i(n+n')\alpha_1} e^{-i(m+m')\gamma_1} = 16\pi^4 c_{00}^{\Theta,n',m'} \delta_{n,-n'} \delta_{m,-m'}. \end{aligned} \tag{A8}$$

Result (A1) follows immediately from (A3) and (A8).

APPENDIX B: LEGENDRE POLYNOMIAL ORIENTATIONAL CORRELATION TIMES FOR RESTRICTED ANGULAR DIFFUSION

The lth order orientational correlation time, $\tau_{\mathrm{eff}}^{(l)}$, is defined by

$$\tau_{\mathrm{eff}}^{(l)}\left(1-S_l^2\right) = \int_0^\infty \left[C_l\left(t\right) - S_l^2\right] \mathrm{d}t. \tag{B1}$$

The correlation time is a fundamental quantity which can be compared for any fit or model of the correlation function. Lipari and Szabo exactly determined $\tau_{\mathrm{eff}}^{(2)}\left(1-S_2^2\right)$ (corresponding to the fluorescence or pump-probe anisotropy decay) for the model of diffusion in a hard cone potential, without direct calculation of the correlation function.[17] Their method is general and can be immediately applied to all l; we summarize our adaptation of the procedure in the following.

Let

$$F_{lm}\left(\Omega\right) = C_{lm}\left(\Omega\right) - \delta_{m0} S_l, \tag{B2}$$

with S_l the order parameter and $C_{lm}\left(\Omega\right)$ the modified spherical harmonics.[25,45] The derivation of Lipari and Szabo easily provides[17]

$$D_w \tau_{\mathrm{eff}}^{(l)}\left(1-S_l^2\right) = \sum_{m=-l}^{l} \tau_m^{(l)}, \tag{B3}$$

with D_w the wobbling diffusion constant, and the $2l+1$ terms in the sum given by

$$\tau_m^{(l)} = \int \mathrm{d}\Omega F_{lm}^*\left(\Omega\right) T_{lm}\left(\Omega\right) p_{\mathrm{eq}}\left(\theta\right). \tag{B4}$$

T_{lm} is the solution to the simple differential equation

$$\nabla_\Omega^2 T_{lm}\left(\Omega\right) = -F_{lm}\left(\Omega\right), \tag{B5}$$

with ∇_Ω^2 the angular part of the Laplacian operator, and T_{lm} satisfies the boundary condition

$$\left.\frac{\partial}{\partial\theta} T_{lm}\left(\Omega\right)\right|_{\theta=\theta_0} = 0, \tag{B6}$$

with θ_0 the cone half angle. Furthermore, because $\tau_m^{(l)} = \tau_{-m}^{(l)}$, we need to only obtain T_{lm} for $m = 0, 1, \ldots, l$.[17]

First, we address the $m = 0$ case. Henceforth, we shall make use of the angular coordinates Ω defined by $(x = \cos\theta, \phi)$, with $x_0 = \cos\theta_0$. Equation (B5) becomes

$$\frac{\partial}{\partial x}\left(1-x^2\right)\frac{\partial}{\partial x} T_{l0}\left(x\right) = -P_l\left(x\right) + S_l. \tag{B7}$$

This is easily solved by direct integration, with boundary conditions (B6) and that the solution is well-behaved at $x = 1$. The overall constant term after the second integration is arbitrary as it does not affect (B4); we can choose it such that $T_{l0}\left(x=1\right) = 0$ for definitiveness. It is easy to show that $p_{\mathrm{eq}}\left(x\right) = 1/\left(2\pi\left(1-x_0\right)\right)$ for $x > x_0$, and $p_{\mathrm{eq}}\left(x\right) = 0$ otherwise.[17] Therefore,

$$\tau_0^{(l)} = \int \mathrm{d}\Omega F_{l0}^*\left(\Omega\right) T_{l0}\left(\Omega\right) p_{\mathrm{eq}}\left(x\right) = \frac{1}{1-x_0}\int_{x_0}^1 \mathrm{d}x F_{l0}^*\left(x\right) T_{l0}\left(x\right) = \frac{1}{1-x_0}\int_{x_0}^1 \mathrm{d}x \left(P_l\left(x\right) - S_l\right) T_{l0}\left(x\right), \tag{B8}$$

following directly from the ϕ invariance of the integrand.

The remaining case is $0 < m \le l$. We define

$$T_{lm}\left(\Omega\right) = \left(-1\right)^m \frac{e^{im\phi}}{l\left(l+1\right)}\left[\frac{\left(l-m\right)!}{\left(l+m\right)!}\right]^{1/2} K_{lm}\left(x\right), \tag{B9}$$

which, upon substitution into (B5), gives

$$\frac{\partial}{\partial x}\left(1-x^2\right)\frac{\partial}{\partial x} K_{lm}\left(x\right) - \frac{m^2}{1-x^2} K_{lm}\left(x\right) = -l\left(l+1\right) P_l^m\left(x\right), \tag{B10}$$

with P_l^m an associated Legendre function. Clearly, $K_{lm}\left(x\right)$ must satisfy the same boundary conditions as $T_{lm}\left(\Omega\right)$. We substitute (B9) into (B4) and, recalling that $F_{lm} = C_{lm}$ for $m > 0$, we can trivially perform the ϕ integration to obtain

$$\tau_m^{(l)} = \frac{\left(l-m\right)!}{l\left(l+1\right)\left(l+m\right)!\left(1-x_0\right)}\int_{x_0}^1 \mathrm{d}x P_l^m\left(x\right) K_{lm}\left(x\right). \tag{B11}$$

All that remains is the determination of K_{lm}. The particular solution $K_{lm}\left(x\right) = P_l^m\left(x\right)$ clearly holds, because then (B10)

is simply the associated Legendre differential equation. The complete solution will consist of the sum of this particular solution and any factor of the general solution to the associated homogeneous equation of (B10). The general solution to the homogeneous equation, which is well-behaved at $x = 1$, is[17]

$$K_{lm}(x) = \frac{1}{2m}\left(\frac{1-x}{1+x}\right)^{m/2}. \tag{B12}$$

The particular linear combination of P_l^m and (B12) is chosen to ensure that K_{lm} satisfies boundary condition (B6). The results of these calculations for $l = 1,\ldots,4$ appear in Table II in the main text.

We point out that in the original derivation of the $l = 2$ wobbling correlation time in Appendix A in Ref. 17 two of the intermediate results, Eqs. (A25) and (A26), are incorrect. However, the final result, Eq. (24) of Lipari and Szabo in the main text (reproduced in Table II), is indeed recovered by following either their procedure[17] or the adaptation presented in this appendix. Corresponding to Eq. (A25) in Ref. 17, we obtain for $l = 2$ and $m = 1$ the intermediate expression

$$K_{21}(x) = -3x\sqrt{1-x^2} + \frac{3\left(\frac{1-x_0}{1+x_0}\right)^{1/2}(1+x_0)^2\left(2x_0^2-1\right)\left(\frac{1-x}{1+x}\right)^{1/2}}{\sqrt{1-x_0^2}}, \tag{B13}$$

which is well behaved at $x = 1$ and satisfies boundary condition (B6). Similarly, corresponding to Eq. (A26) of Lipari and Szabo,[17] our intermediate expression for $l = 2$ and $m = 2$ is

$$K_{22}(x) = 3\left(1-x^2\right) - 3x_0(1+x_0)^2\left(\frac{1-x}{1+x}\right), \tag{B14}$$

again satisfying the boundary conditions.

Small θ_0 approximations to $\tau_{\text{eff}}^{(l)}$ were constructed from the first two non-zero terms in the power series expansion around $\theta_0 = 0$. The cone half angles for which the approximate correlation time is in error by 10% compared to the exact time are 96° for $l = 1$, 77° for $l = 2$, 63° for $l = 3$, and 52.5° for $l = 4$.

[1]P. Hamm and M. T. Zanni, *Concepts and Methods of 2D Infrared Spectroscopy* (Cambridge University Press, Cambridge, New York, 2011).
[2]S. Park, K. Kwak, and M. D. Fayer, Laser Phys. Lett. **4**, 704–718 (2007).
[3]K. Kwak, S. Park, I. J. Finkelstein, and M. D. Fayer, J. Chem. Phys. **127**, 124503 (2007).
[4]K. Kwak, D. E. Rosenfeld, and M. D. Fayer, J. Chem. Phys. **128**, 204505 (2008).
[5]S. Park, D. E. Moilanen, and M. D. Fayer, J. Phys. Chem. B **112**, 5279–5290 (2008).
[6]S. T. Roberts, J. J. Loparo, and A. Tokmakoff, J. Chem. Phys. **125**, 084502 (2006).
[7]E. T. J. Nibbering and T. Elsaesser, Chem. Rev. **104**, 1887–1914 (2004).
[8]R. A. Nicodemus, S. A. Corcelli, J. L. Skinner, and A. Tokmakoff, J. Phys. Chem. B **115**, 5604–5616 (2011).
[9]R. A. Nicodemus, K. Ramasesha, S. T. Roberts, and A. Tokmakoff, J. Phys. Chem. Lett. **1**, 1068–1072 (2010).
[10]S. Mukamel, *Principles of Nonlinear Optical Spectroscopy* (Oxford University Press, New York, 1995).
[11]Q. Guo, P. Pagano, Y.-L. Li, A. Kohen, and C. M. Cheatum, J. Chem. Phys. **142**, 212427 (2015).
[12]P. L. Kramer, J. Nishida, C. H. Giammanco, A. Tamimi, and M. D. Fayer, J. Chem. Phys. **142**, 184505 (2015).
[13]C. A. Rivera, A. J. Souna, J. S. Bender, K. Manfred, and J. T. Fourkas, J. Phys. Chem. B **117**, 15875–15885 (2013).
[14]R. B. Williams, R. F. Loring, and M. D. Fayer, J. Phys. Chem. B **105**, 4068–4071 (2001).
[15]G. U. Bublitz and S. G. Boxer, Annu. Rev. Phys. Chem. **48**, 213–242 (1997).
[16]C. C. Wang and R. Pecora, J. Chem. Phys. **72**, 5333–5340 (1980).
[17]G. Lipari and A. Szabo, Biophys. J. **30**, 489–506 (1980).
[18]P. L. Kramer, C. H. Giammanco, and M. D. Fayer, J. Chem. Phys. **142**, 212408 (2015).
[19]P. L. Geissler, Annu. Rev. Phys. Chem. **64**, 317–337 (2013).
[20]Z. L. Terranova and S. A. Corcelli, J. Phys. Chem. B **118**, 8264–8272 (2014).
[21]S. Corcelli and J. L. Skinner, J. Phys. Chem. A. **109**, 6154–6165 (2005).
[22]S. Corcelli, C. P. Lawrence, and J. L. Skinner, J. Chem. Phys. **120**, 8107–8117 (2004).
[23]C. P. Lawrence and J. L. Skinner, J. Chem. Phys. **118**, 264–272 (2003).
[24]K. P. Sokolowsky, H. E. Bailey, and M. D. Fayer, J. Chem. Phys. **141**, 194502 (2014).
[25]R. N. Zare, *Angular Momentum* (Wiley-Interscience, 1988).
[26]B. J. Berne and R. Pecora, *Dynamic Light Scattering* (Dover, Mineola, New York, 2000).
[27]H.-S. Tan, I. R. Piletic, and M. D. Fayer, J. Opt. Soc. Am. B **22**, 2009–2017 (2005).
[28]Y. L. A. Rezus and H. J. Bakker, J. Chem. Phys. **123**, 114502 (2005).
[29]M. Cho, G. R. Fleming, and S. Mukamel, J. Chem. Phys. **98**, 5314–5326 (1993).
[30]A. Tokmakoff, J. Chem. Phys. **105**, 1–12 (1996).
[31]K. Kinosita, A. Ikegami, and S. Kawato, Biophys. J. **37**, 461–464 (1982).
[32]K. Kinosita, S. Kawato, and A. Ikegami, Biophys. J. **20**, 289–305 (1977).
[33]G. Lipari and A. Szabo, J. Am. Chem. Soc. **104**, 4546–4559 (1982).
[34]D. B. Spry, A. Goun, K. Glusac, D. E. Moilanen, and M. D. Fayer, J. Am. Chem. Soc. **129**, 8122–8130 (2007).
[35]K. Ramasesha, S. T. Roberts, R. A. Nicodemus, A. Mandal, and A. Tokmakoff, J. Chem. Phys. **135**, 054509 (2011).
[36]H.-S. Tan, I. R. Piletic, and M. D. Fayer, J. Chem. Phys. **122**, 174501 (2005).
[37]F. W. Deeg, J. J. Stankus, S. R. Greenfield, V. J. Newell, and M. D. Fayer, J. Chem. Phys. **90**, 6893 (1989).
[38]D. McMorrow, W. T. Lotshaw, and G. A. Kenney-Wallace, IEEE J. Quantum Electron. **24**, 443–454 (1988).
[39]A. L. Sturlaugson, A. Y. Arima, H. E. Bailey, and M. D. Fayer, J. Phys. Chem. B **117**, 14775–14784 (2013).
[40]A. L. Sturlaugson, K. S. Fruchey, and M. D. Fayer, J. Phys. Chem. B **116**, 1777–1787 (2012).
[41]D. E. Moilanen, E. E. Fenn, Y. S. Lin, J. L. Skinner, B. Bagchi, and M. D. Fayer, Proc. Natl. Acad. Sci. U. S. A. **105**, 5295–5300 (2008).
[42]H. Shirota, T. Mandai, H. Fukazawa, and T. Kato, J. Chem. Eng. Data **56**, 2453–2459 (2011).
[43]K. R. Harris, M. Kanakubo, and L. A. Woolf, J. Chem. Eng. Data **52**, 1080–1085 (2007).
[44]J. Nishida and M. D. Fayer, J. Chem. Phys. **140**, 144702 (2014).
[45]D. M. Brink and G. R. Satchler, *Angular Momentum*, 2nd ed. (Oxford University Press, Oxford, 1968).